NE 795: Advanced Reactor Materials

Fall 2023

Dr. Benjamin Beeler

Exam Results

- Avg: 92.25 ; added a 2.75 point curve

Last Time

- Constituent redistribution in UZr
  - thermodynamic and Soret diffusion effects
- Different porosities in different phases
- Thermal conductivity degrades with porosity, but increases with sodium infiltration
- Fuel cladding mechanical and chemical interaction
- FCMI limited by low smear density and large plenum
  - swelling due to fission gas and solid fission products
- FCCI is a complex thermodynamic and kinetic process
  - low melting phases can be studied with diffusion couples

Paper Presentations

- Two options:
  - Current: 4 tests (16% each); 2 presentations (18% each)
    - second presentation will likely be last day of classes, or during the finals slot
  - Alternate: 4 tests (20% each); 1 presentation (20%)
    - first presentation during normal class hours, but will be slightly more extensive

Presentation 1 topic assignments:

- Mohamed Abdulhameed
  - Inert matrix actinide-bearing fuel concepts
- Nermeen Elamrawy
  - SiC as a cladding material (non-TRISO applications)
- ATM Jahid Hasan
  - High temperature materials for gas reactor heat exchangers
- Lucia Gomez Hurtado
  - The role and effect of silver in SiC
- Shehab Shousha
  - Swelling of stainless steel under fast fluence

FCCI

- The burnup of a fuel pin is another parameter that impacts the size of the fuel–cladding interaction zone
- Larger interaction zones are observed for higher burnup fuel elements
- The larger inventories of fission products allow more lanthanides to diffuse down the temperature gradient, thereby increasing the inventory of fission products at the interface
- For high burnup fuels, temperature effects also exacerbate FCCI due to thermal cond. degradation producing higher temperatures, and more rapid FP diffusion
- Fuel elements at the hotter core positions can exhibit increased interdiffusion at the fuel–cladding interface over those at colder positions

FCCI Compositions

- Fe and Cr are the major constituents in HT-9 cladding and should show up as major constituents in the FCCI zones of irradiated HT-9-clad fuel elements
- For D9-clad fuel elements, Fe, Ni, and Cr are major constituents that should be present in FCCI zones
- There have been some irradiated fuel samples that were specifically destructively analyzed to observe FCCI
- The lowest and highest determined temperatures at the fuel–cladding interface were 540 and 660 C, respectively
- The thickest interaction zone measured was 170 μm, and the lanthanide fission products were the primary fuel constituents observed in the interaction layers

Table 1 Nominal compositions for stainless steel cladding materials (wt%)[a]

	HT9	*D9*	*316*
Ni	0.5	15.5	10–14
Cr	12.0	13.5	16–18
Mn	0.2	2.0	2 (max)
Mo	1.0	2.0	2–3
Si	0.25	0.75	1 (max)
Ti	–	0.25	–
C	0.2	0.04	0.08 (max)
W	0.5	–	–
V	0.5	–	–
S	–	–	0.03 (max)
P	–	–	0.045 (max)

FCCI Examinations

Fuel element ID	*Cladding material*	*Fuel composition (at.%)*	*Burnup (at.%)*	*Temperature at fuel–clad interface at BOL (°C)*[a]	*Maximum zone thickness observed (μm)*	*Type of analysis*	*Components originating in the fuel that are found in cladding layers*
DP-81	HT-9	U–23Zr	5.0	660	70	EPMA	Ce, Pr, Nd
DP-11	HT-9	U–23Zr	10.0	660	90	EPMA	Ce, Pr, Nd, La, Sm, Pd
DP-04	HT-9	U–23Zr	10.0	660	90	EPMA	Ce, Pr, Nd, La, Sm, Pd
DP-70[b]	HT-9	U–23Zr	10.0	660	140	EPMA	Ce, Pr, Nd, La, Sm, Pd
DP-75	HT-9	U–23Zr	10.0	660	170	EPMA	Ce, Pr, Nd, La, Sm, Pd
T459	HT-9	U–16Pu–23Zr	3.0	ND[c]	10	EPMA	Ce, Pr, Nd
DP-16(1)	HT-9	U–16Pu–23Zr	9.7	540	40	SEM	Ce, Nd, La, U, Pu, Pd
DP-16(2)	HT-9	U–16Pu–23Zr	10.1	550	40	EPMA	Ce, Nd, Pr, Pu
DP-21	HT-9	U–16Pu–23Zr	11.4	ND	ND	EPMA	ND
C709	D9	U–23Zr	9.3	650	111	EPMA	Ce, Nd, La
T225	D9	U–23Zr	10.0	ND	25	OM	ND
T141	D9	U–23Zr	11.9	ND	17	OM	ND
T-159	D9	U–16Pu–23Zr	3.0	ND	ND	EPMA	Ce, Pr, Nd, Pu
[d]	D9	U–16Pu–23Zr	6.0	ND	75	EPMA	Ce, Pr, Nd, La
T042	D9	U–7Pu–23Zr	6.0	540	20	EPMA	Ce, Pr, Nd, La
T-087	D9	U–16Pu–23Zr	10.0	ND	50	EPMA	Ce, Pr, Nd, La, Pu
A-850	D9	U–16Pu–23Zr	10.1	550	100	EPMA	Ce, Nd, La, Pu
T-112	D9	U–16Pu–23Zr	11.9	ND	72	EPMA	ND
T-106	D9	U–16Pu–23Zr	17.0	ND	20	EPMA	Ce, Pr, Nd, La
T341	316SS	U–16Pu–23Zr	0.4	ND	ND	EPMA	ND

FCCI Compositions

- Element DP-16 was the only fuel element in which a sample was generated for analysis using SEM/EDS, in addition to the more typical OM and EPMA analyses usually performed on fuel elements
- U-16Pu-23Zr and HT-9 cladding
- X-ray analysis maps at the right

DP-16(1)	HT-9	U–16Pu–23Zr	9.7	540	40	SEM	Ce, Nd, La, U, Pu, Pd
DP-16(2)	HT-9	U–16Pu–23Zr	10.1	550	40	EPMA	Ce, Nd, Pr, Pu

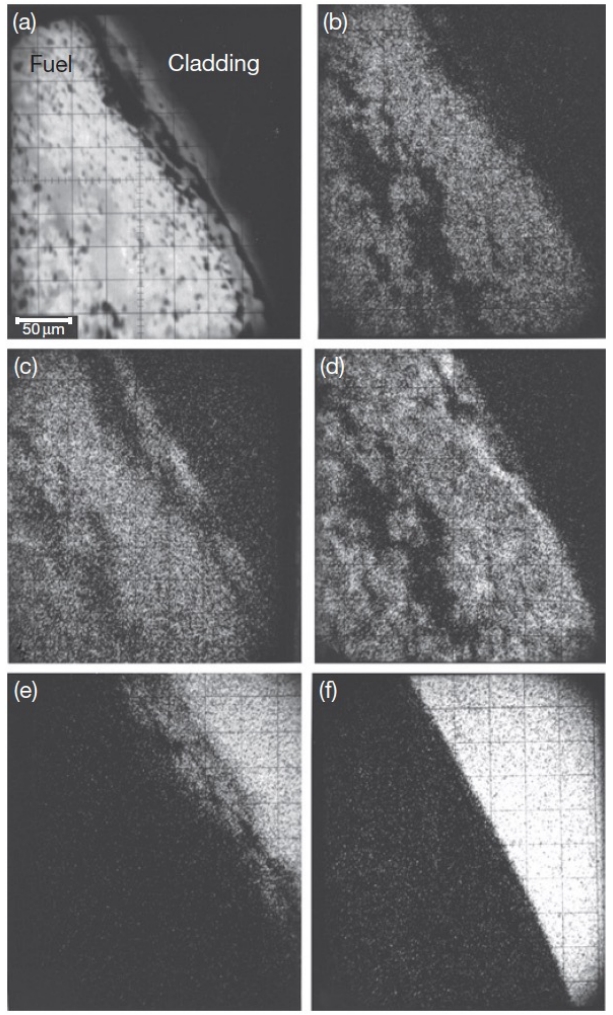

(b) U,
(c) Pu,
(d) Zr,
(e) Fe,
(f) Cr

FCCI Compositions

- X-ray map for fission products
- EPMA analysis for key species
- Fe diffuses into the fuel, Ce and Nd diffuse into the cladding, and Pd enriches in localized areas of the fuel near the fuel–cladding interface
- The lanthanides penetrated the farthest into the cladding (40 mm) of any components originating in the fuel

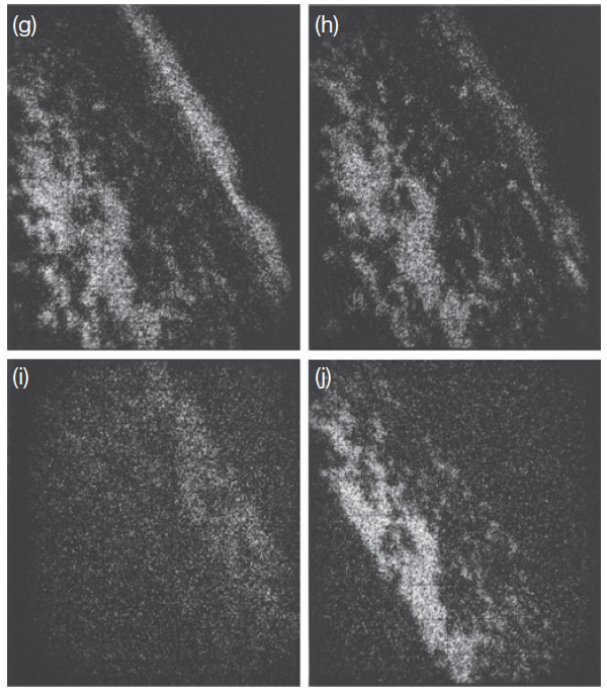

(g) Ce, (h) Nd, (i) Ru, and (j) Pd

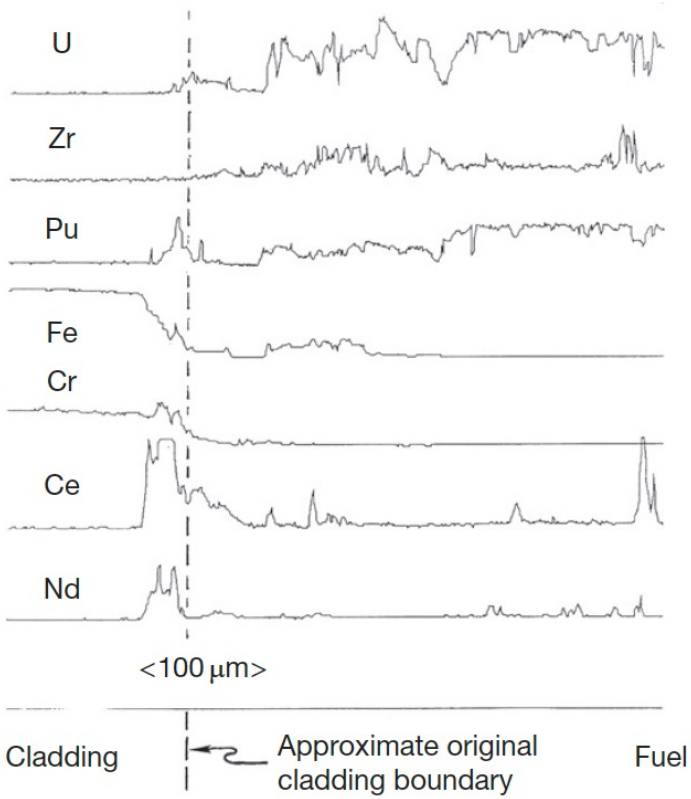

FCCI Compositions

- The DP-11 fuel element was irradiated to about 10 at.% burnup at elevated cladding temperatures (630–660 C), binary U-Zr
- There is a 50-μm-wide zone of the cladding that is high in Cr and low in Fe and Ni
- In the fuel, Fe has interdiffused around 250 μm
- In the cladding band containing high Cr and low Fe and Ni, lanthanide concentrations are elevated

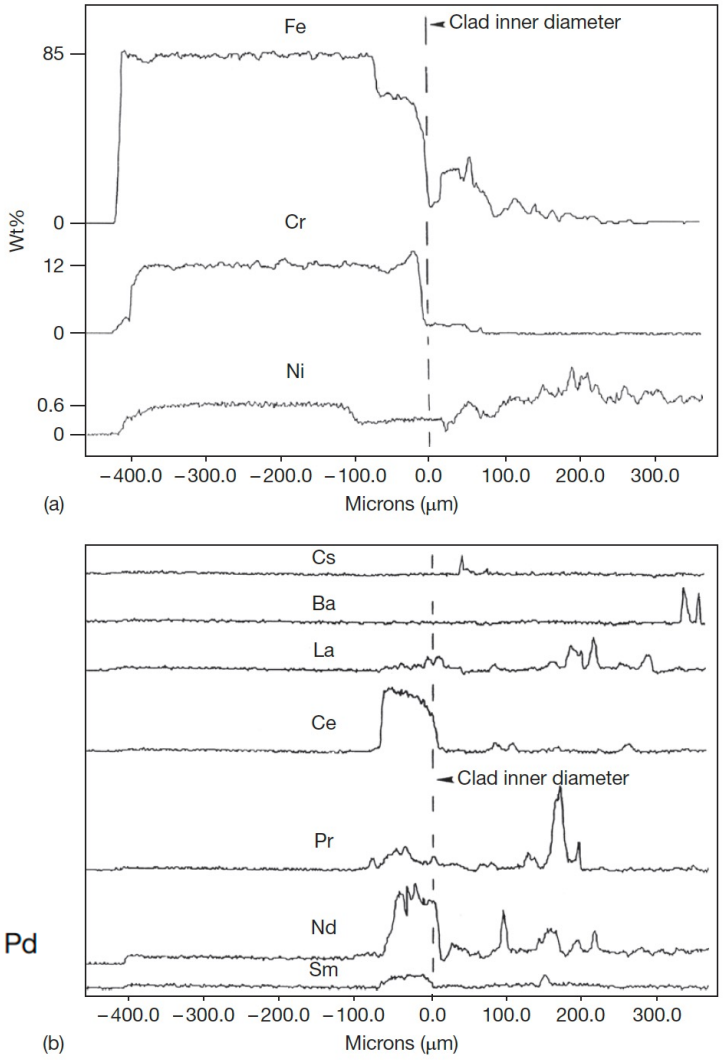

DP-11	HT-9	U–23Zr	10.0	660	90	EPMA	Ce, Pr, Nd, La, Sm, Pd

FCCI

- A variety of phases have been observed to form locally where swelled fuel has contacted the cladding
- At the interface between the fuel and the cladding, the observed phases on both sides combine the cladding elements Fe, Ni, and Cr with the fuel components U, Zr, and Pu and the lanthanide fission products
- In the cladding, the developed phases are enriched with cladding components, and they contain differing amounts of the primary fuel components and fission product components
- Lanthanides penetrate farthest into the cladding, specifically Ce and Nd
- Fe and Ni depletion zones are observed in all the fuel elements

FCCI

- In the fuel, some phases are observed that are enriched with the fuel constituents and contain Fe or Ni as the major nonfuel or components
- Other phases are observed that primarily contain lanthanides
- The interaction zone formation is localized
- Temperature and power variations along the length of a fuel element appear to impact the amount of FCCI that occurs

Two different locations in DP-16

Layer	Fe	Cr	Si	Pd	Ce[b]	Nd[b]	Zr	Pu	Other[b]
1	2	2	0	24	16	34	19	1	–
1	1	1	5	35	19	33	5	1	–
1	–	–	5	38	13	26	7	2	9La
1	–	–	–	20	10	16	31	–	6La, 17Pb
2	–	34	6	–	11	23	–	–	3Mo, 6La, 8U, 9Sn
2	2	28	7	–	16	28	–	–	La, 7U, 1Ag, 10Sn
3	28	20	5	15	10	12	–	11	–
4	63	10	4	–	7	13	–	0.3	1La
4	66	15	6	–	5	7	–	0.2	1Ag
4	67	13	6	–	5	7	–	0.2	1Ag
4	69	16	4	–	5	5	–	0.3	1Ag

Layer	Fe	Cr	Mo	Si	Pu	U	Ce	Nd	La	Other
1	41	–	–	2	15	–	10	21	4	7Pd
1	66	2	–	7	22	–	2	2	2	1Ni, 1Ba
1	55	14	0.4	2	3	1	7	15	2	0.4Ni
2	–	28	1	–	5	4	15	39	6	–
3	37	39	2	2	8	2	5	3	1	0.5Mn
4	69	17	–	1	0.2	–	5	6	–	1Mn, 0.4Ni

Melting Experiments

- One potentially significant impact that the presence of FCCI zones is the melting of phases inside the cladding
- This will limit the allowable coolant temperature that can be used for the reactor, but it can become more important when considering transients and accidents
- This illustrates the effect of the relatively low quantities of Fe required to cause melting on the uranium-rich side of the U–Fe phase diagram
- In general, no liquid phase formation is observed below heating at 700C

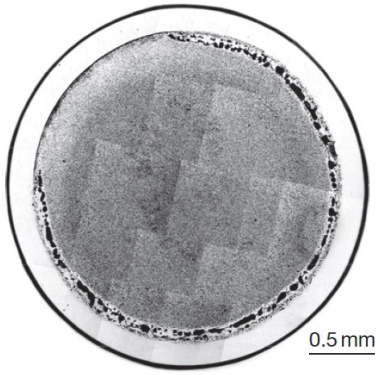

Figure 11 FBTA test result showing an HT-9 clad U–10 wt% Zr fuel pin segment (~3 at.% BU) after being heated at 750 °C for 1 h.

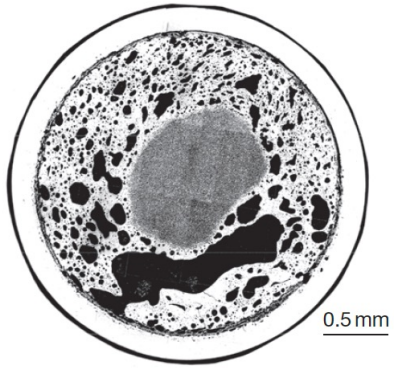

Figure 12 FBTA test result showing an HT-9 clad U–10 wt% Zr fuel pin segment (~3 at.% BU) after being heated at 800 °C for 1 h. Note that all but the fuel center has been at least partially melted, and the cladding has not been fully penetrated.

METAL FUEL FABRICATION

Metal Fuel Fabrication

- Injection casting has been utilized for fuel slug fabrication
- Remote fabrication has been performed inside a hot cell on recovered uranium
- Fuel slugs for EBR II and FFTF were fabrication via injection casting

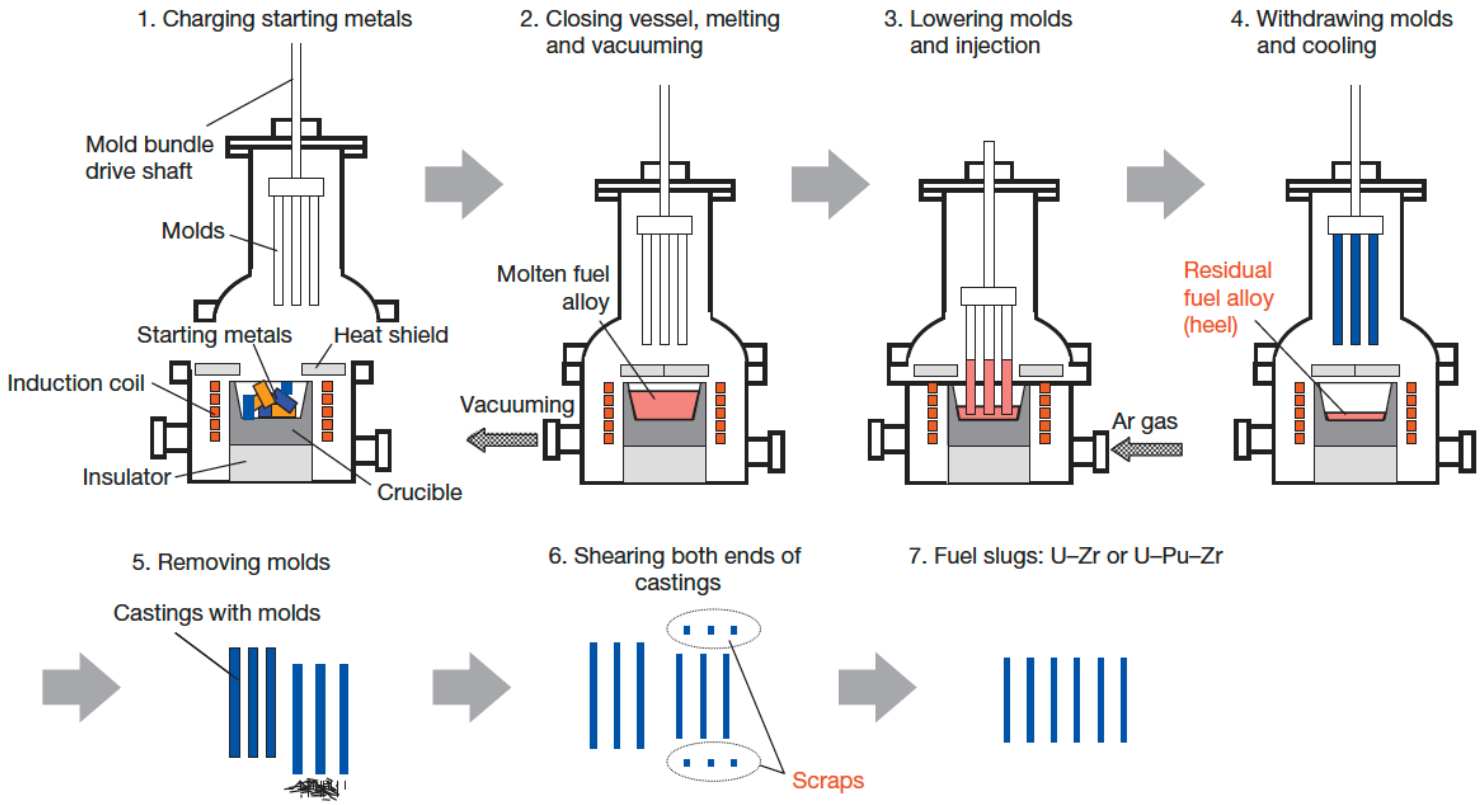

Metal Fuel Fabrication

- Starting materials are charged into the graphite crucible in the furnace
- Silica molds with tops closed are set above the crucible
- Crucible is coated with yttria
- Molds coated with zirconia

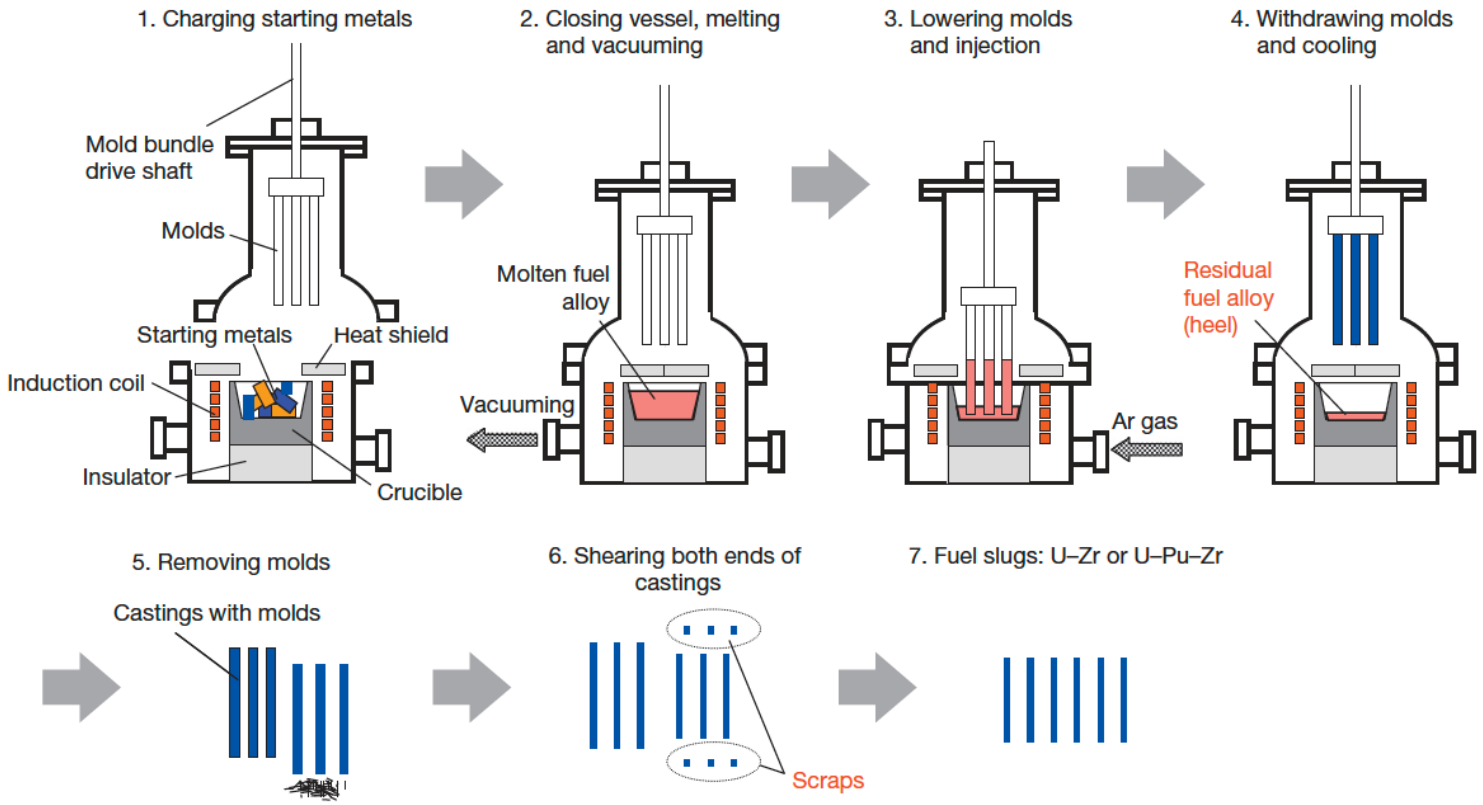

Metal Fuel Fabrication

- Furnace closed and filled with Ar gas
- Crucible is inductively heated to 1830K, and stirred electromagnetically
- Ar gas removed, molds are lowered, then Ar gas returned
- Pressure difference injects the melt into the molds

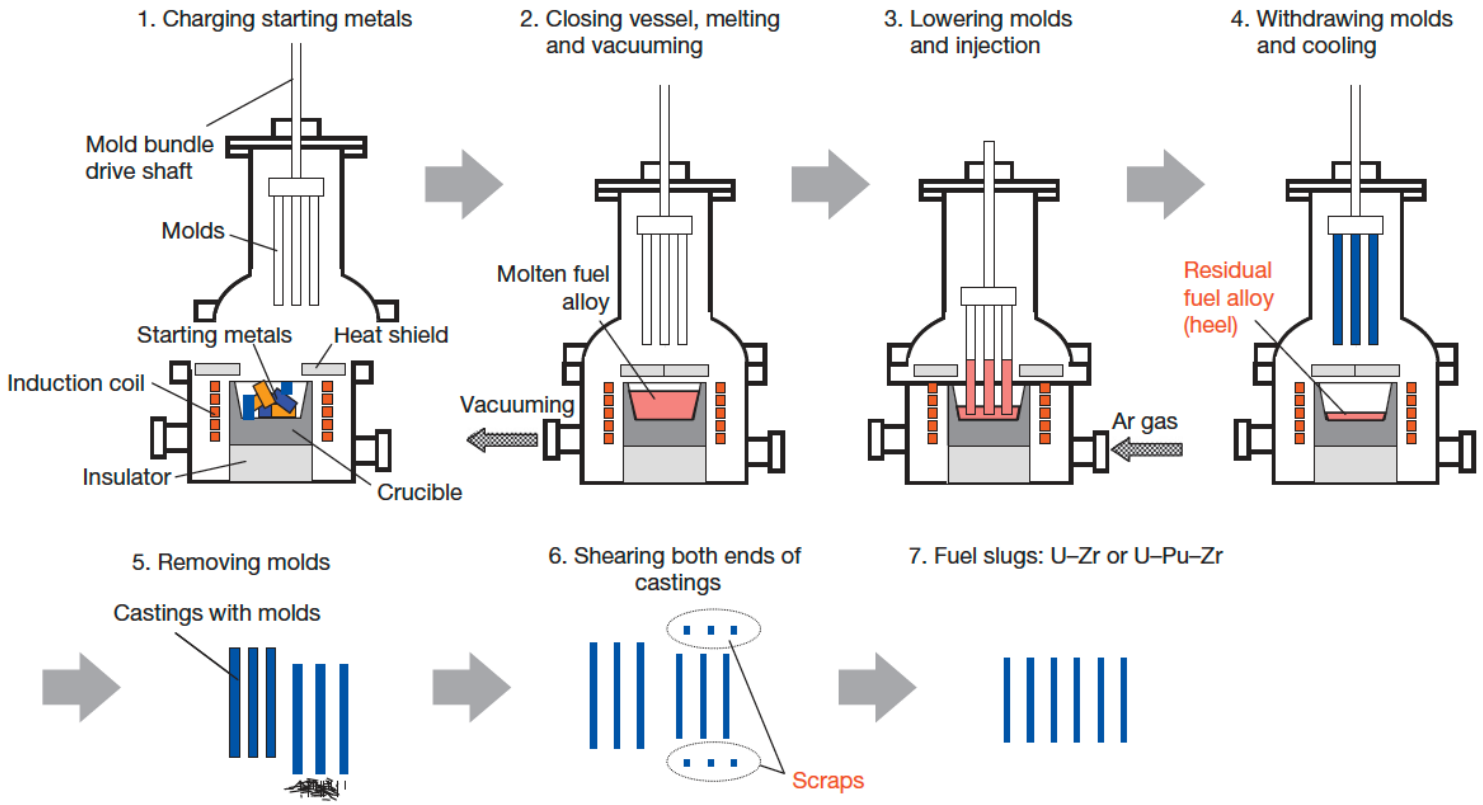

Reprocessing

- Pyroprocessing
- For more than 50 years, pyrometallurgy has been studied as an alternative strategy in the reprocessing of used fuel
- Pyrochemical processes rely on refining techniques at high temperature (500–900 C) depending on the molten salt eutectic used
- Typically, chloride systems operate at lower temperature compared to fluoride systems, and are preferred in processing
- These processes are mainly based on electrorefining or on extraction from the molten salt phase into liquid metal
- Two processes-one for oxide fuel and one for metallic fuel-have been developed to near industrial scale

IFR Pyroprocess

- This process was developed in the US to be part of the IFR project, and can handle the treatment of transuranics
- The fuel is recycled using an electrochemical process based on molten chloride salts and liquid metals
- The molten salt medium for electrorefining is a solution of a certain amount of UCl3 dissolved in a LiCl–KCl eutectic

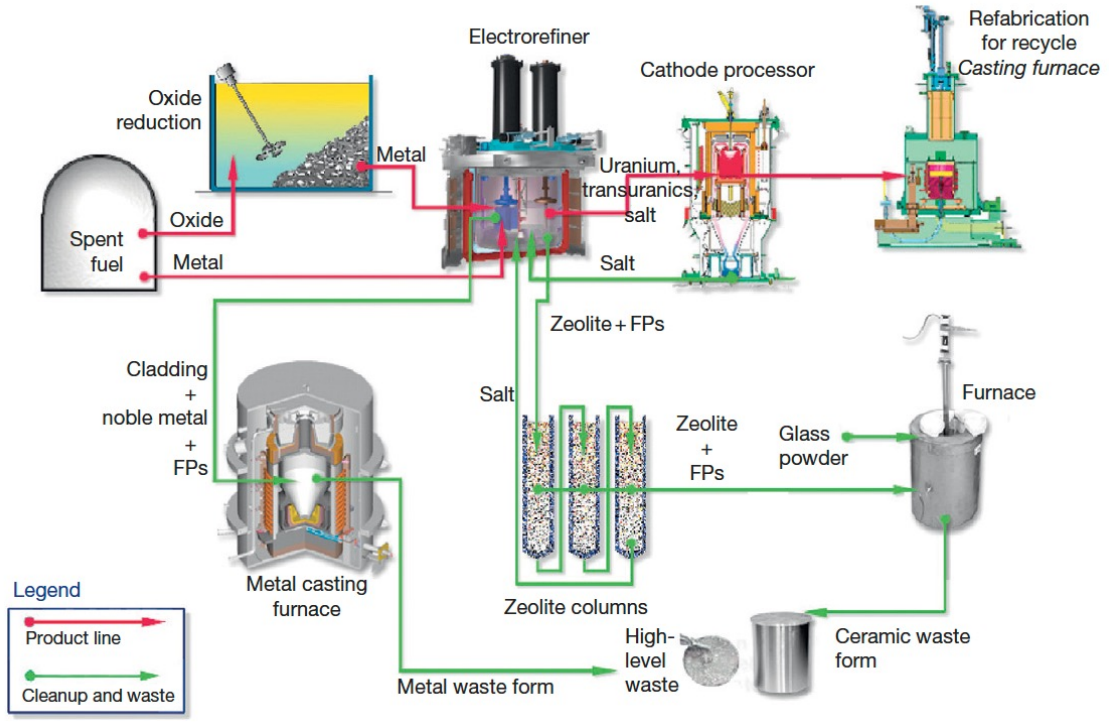

IFR Pyroprocess

- The fuel is electrochemically dissolved using a potential between the basket (loaded with used fuel) as anode and a stainless steel electrode in the salt as the cathode
- Uranium and TRU are deposited on the cathodes
- Once the fuel is dissolved and most of the uranium is deposited on the solid steel, this cathode is replaced by a liquid cadmium cathode, and the remaining TRUs can be co-deposited with the remaining uranium

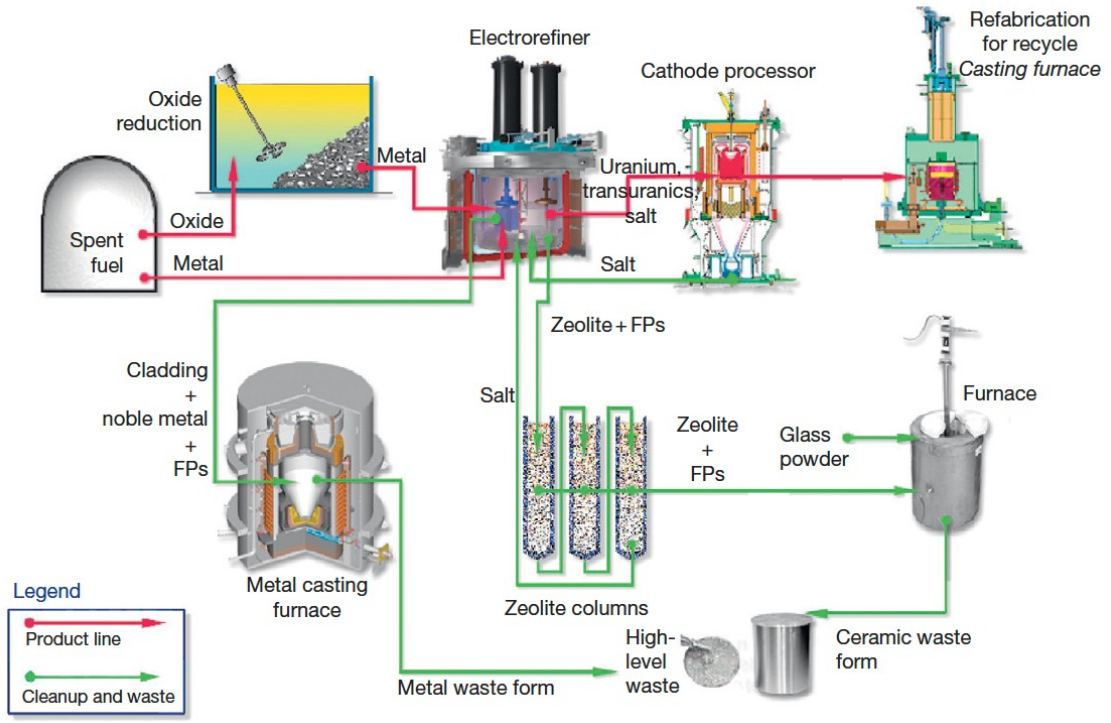

IFR Pyroprocess

- The alkali, alkaline earth, rare earth, and halide FPs remain primarily dissolved in the salt phase
- More than 90% of the noble metal FPs and fuel alloy material are retained in the chopped fuel cladding segments in the anode baskets
- Can reduce the repository burden of radioactive waste by separating long-lived MA from spent light-water reactor fuel, burning MA in fast reactors, and decreasing the long-term radioactivity of nuclear waste

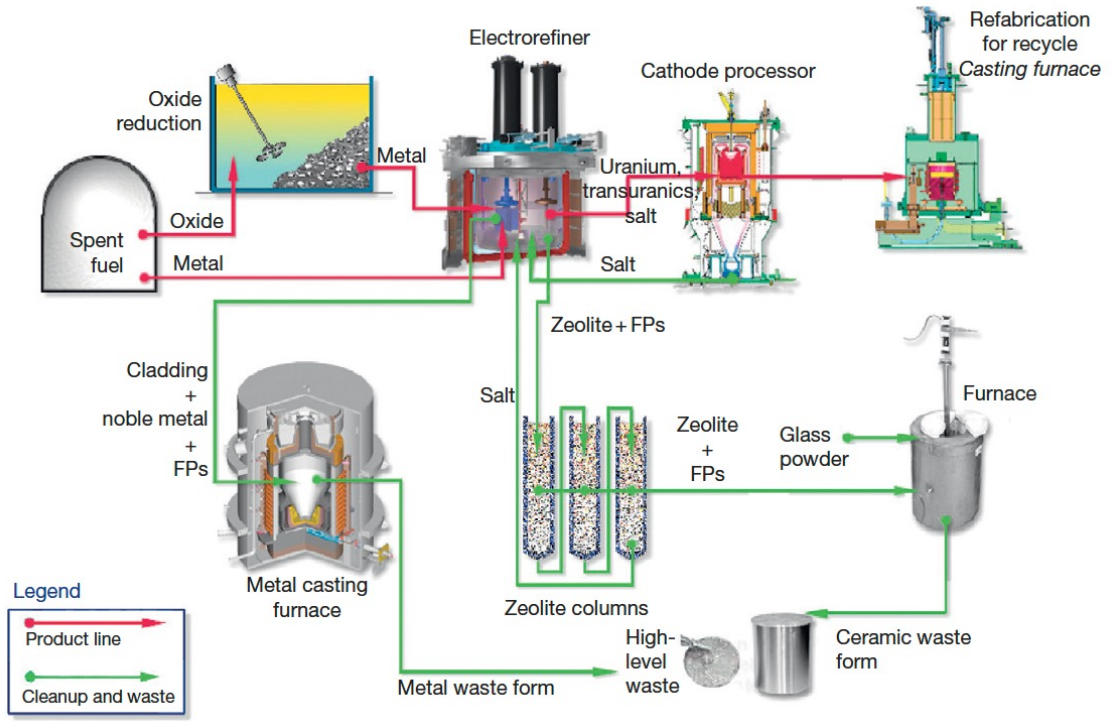

Refabrication

- Metal-fueled fast reactors facilitate the effective transmutation of MA because of the high-energy neutron spectrum
- One of the measures to load MA into the reactor core is to add MA to the fuel alloy homogeneously
- Can perform injection casting in the same manner as the fresh fuel, to form MA-bearing fuel alloys
- These technologies are expected to reduce the fuel cycle cost even for small-scale fuel cycle plants because of the simplicity of the process and the compactness of the equipment
- For example, in the injection casting process, composition adjustment, melting (alloying), and casting of the fuel slug can be done in a single injection-casting furnace

METALLIC FUEL PERFORMANCE MODELING

Metallic Fuel Phenomena

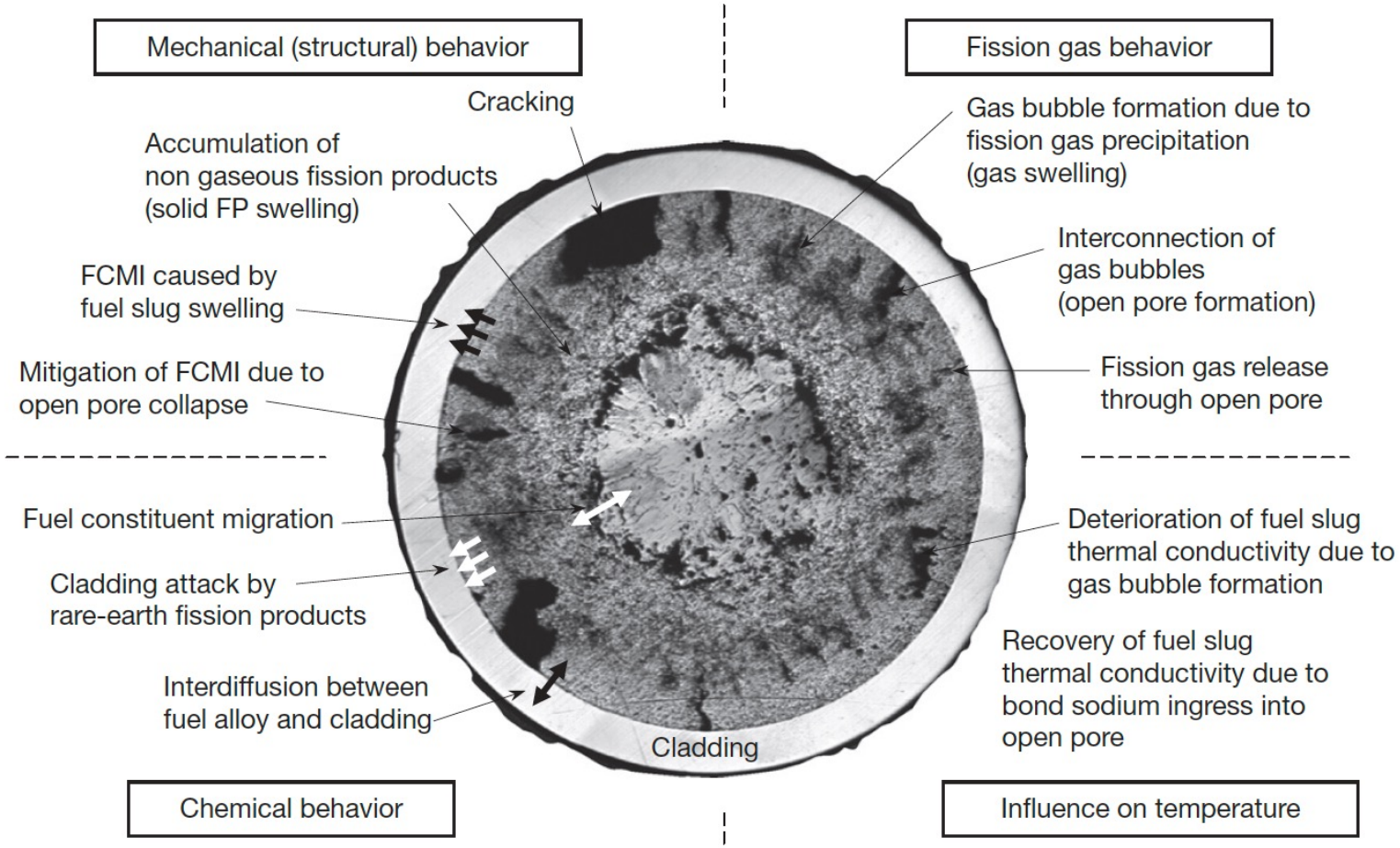

Constituent Redistribution Models

- Constituent redistribution is driven by:
  - temperature gradients in the fuel,
  - solubility gradients in a phase and phase boundaries,
  - additional chemical potentials applied by fuel–cladding gap and cladding
- Results in three concentric zones, namely, a Zr-enriched central zone, a Zr-depleted and U-enriched intermediate zone, and a slightly Zr-enriched zone on the outer periphery
- Migration quickly levels off early in life after a new distribution settles

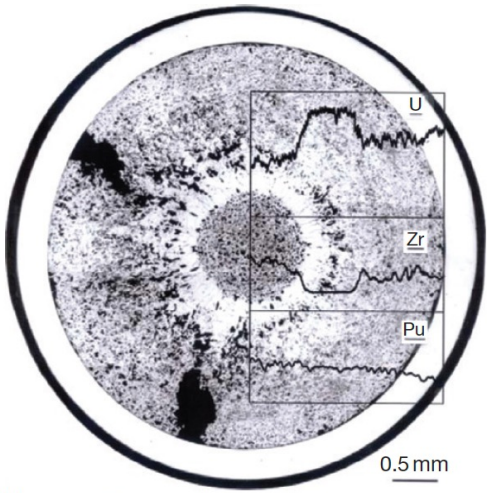

(a) T179 irradiated to 2% burnup

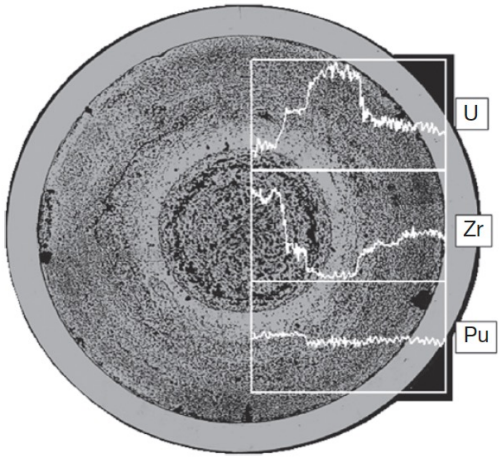

(b) DP-16 irradiated to 11% burnup

Constituent Redistribution Models

- While ternary phase diagrams exist, their accuracy is suspect, and simplified pseudo-binary phase diagrams can be more easily implemented, and removes complexities associated with largely unknown phases
- When applied to a fuel with different Pu content, the phase diagram must be modified accordingly

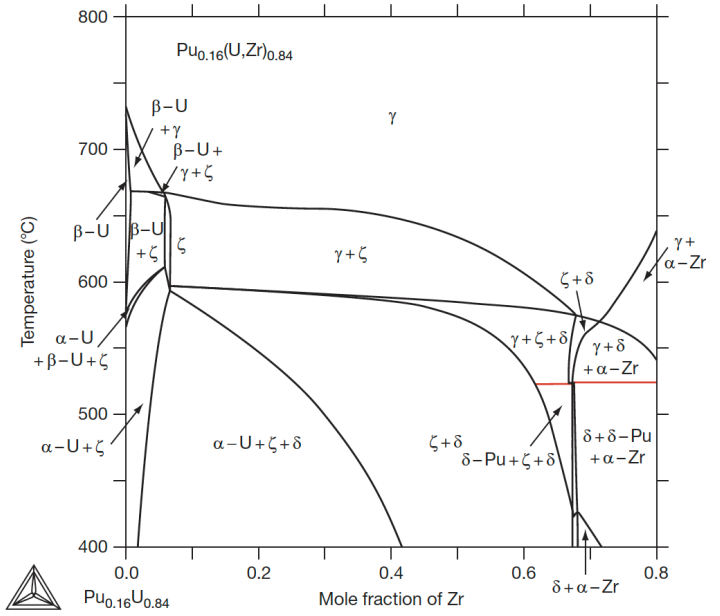

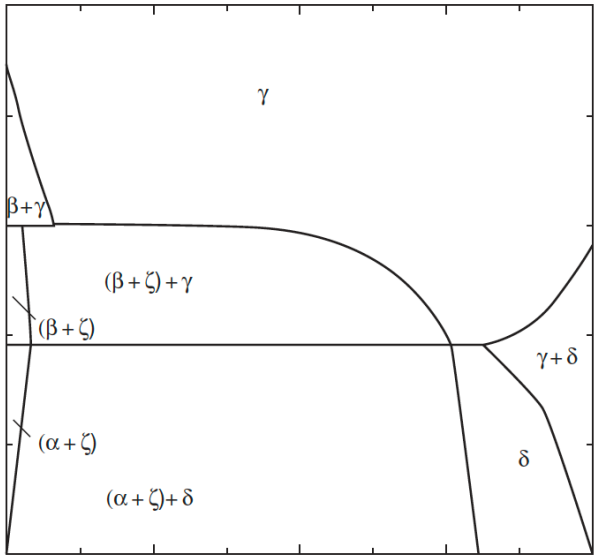

Figure 6 Simplified pseudo-binary phase diagram of U–19Pu–10Zr.

Constituent Redistribution Models

- Using the calculated phase fractions, the Fickian and Soret diffusion coefficient are determined
- Artificial factors are used to set the diffusivity in two-phase regions and to scale diffusivities in each phase
- The magnitudes of diffusivities in each phase are largely unknown, and effectively wholly unknown in two-phase regions

BISON Zr Diffusion Model

$$
\begin{aligned}
D(x,T) &= D_\pi(x,T) \\
S(x,T) &= D_\pi(x,T)\left(\frac{x(1-x_{\mathrm{Pu}}-x)}{1-x_{\mathrm{Pu}}}\right)\frac{Q_\pi^\star}{RT^2} \\
S(x,T) &= f_\beta D_\beta(X_\beta(T),T)\left(\frac{X_\beta(T)(1-x_{\mathrm{Pu}}-X_\beta(T))}{1-x_{\mathrm{Pu}}}\right)\left(\frac{\Delta H_\beta+Q_\beta^*}{RT^2}\right) \\
&\quad +(1-f_\beta)D_\gamma(X_\gamma(T),T)\left(\frac{X_\gamma(T)(1-x_{\mathrm{Pu}}-X_\gamma(T))}{1-x_{\mathrm{Pu}}}\right)\left(\frac{\Delta H_\gamma+Q_\gamma^*}{RT^2}\right)
\end{aligned}
$$

Temperature Predictions

- Constituent redistribution relies on accurate temperature profiles
- Fuel temperature is affected by the thermal conductivity of the fuel, which in turn is changed by porosity evolution and sodium infiltration, in addition to changes in Zr concentration
- BISON thermal conductivity models exist for the distinct phases/species, and account for degradation of thermal conductivity

$$
\begin{aligned}
k_U &= 21.76 + 1.665 \times 10^{-2} T + 5.167 \times 10^{-6} T^2, \\
k_{Pu} &= -8.162 + 4.841 \times 10^{-2} T - 1.614 \times 10^{-5} T^2, \\
k_{c,U-Zr} &= -97.0 + 177.9 f_{Zr} - 95.94 f_{Zr}^2 + 8.351 \times 10^{-3} T \\
&\quad + 2.931 \times 10^{-5} T^2 - 5.694 \times 10^{-3} f_{Zr} T \\
k_{c,Pu} &= -135.8 - 29.89 w_{Pu} + 351.9 w_{Pu}^2 + 0.3571 - 1.186 \times 10^{-4} T^2 - 0.961 w_{Pu} T
\end{aligned}
$$

$$k = f_p k_o$$

$$f_p = \frac{1 - p}{1 + \beta_p p}$$

$$f_{p-Na} = \left[1 - 3 \cdot \frac{1 - k_{Na}/k_f}{2/\varepsilon + (3 - 2/\varepsilon)(k_{Na}/k_f)} \cdot \frac{p_{Na}}{1 - p_g} \right]$$

Porosity Predictions

- BISON utilizes a simplified model for porosity
- The mechanical force balance on an equilibrium bubble can be expressed by the Young-Laplace equation
- Making assumptions for creep stress, bubble size, can calculate swelling due to fission gas
- Finally, can determine porosity from the swelling
- Solid fission products are a function of fission density

$$p = \frac{2\gamma}{r_b} - \sigma_h + \sigma_{cr}$$

$$pV = \nu RT$$

$$V = \frac{\nu RT}{\frac{2\gamma}{r_b} - \sigma_h + \sigma_{cr}}.$$

$$\left(\frac{\Delta V}{V_0}\right)_g = \frac{3.59 \times 10^{-24} FT}{1.01 \times 10^7 - \sigma_h}$$

$$p = \frac{\left(\frac{\Delta V}{V_o}\right)_g}{\left(\frac{\Delta V}{V_o}\right)_g + 1}$$

$$\left(\frac{\Delta V}{V_0}\right)_s = 4.16 \times 10^{-29} F$$

Porosity Predictions

- These porosity models don't incorporate different phases, initial porosity, axial/radial swelling, etc.
- These models have been updated slightly to improve code robustness, but still don't incorporate these critical microstructural phenomena

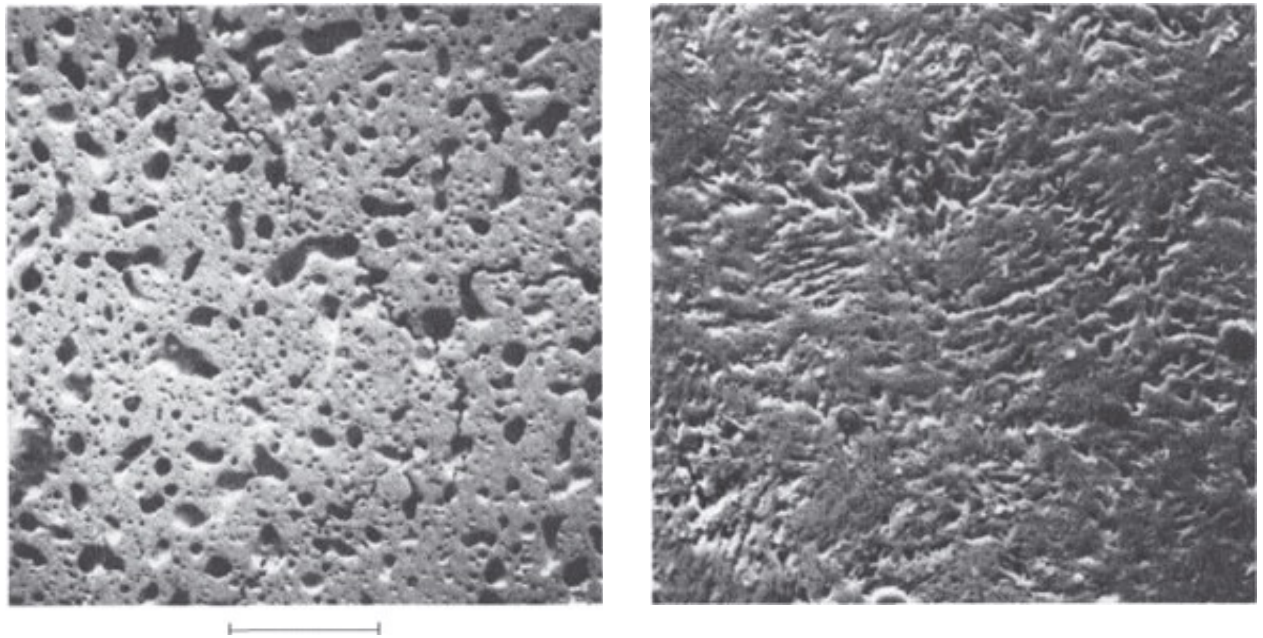

Mechanical Properties

- Young's Modulus

$$E = E_u(1-\beta_E P)\left(\frac{1+0.17W_{Zr}}{1+1.34W_{Zr}} - W_{Pu}\right)\left(1-1.06\left[\frac{T-588}{T_{mu}}\right]\right)$$

- Poisson's ratio

$$\nu = \nu_u(1-\beta_p P)\left(\frac{1+3.4W_{Zr}}{1+1.9W_{Zr}}\right)\left(1+1.2\left[\frac{T-588}{T_{mu}}\right]\right)$$

- Creep

$$\dot{\varepsilon} = A_4\left(1-p^{0.67}\right)^{-3} exp\left(\frac{-Q_3}{RT}\right)\sigma^3 + A_3\dot{F}\sigma$$

- Cladding models for HT-9 creep and k_{th}

$$\dot{\varepsilon}_{cr} = C_5\exp(-\frac{Q_4}{RT})\bar{\sigma}^2 + C_6\exp(-\frac{Q_5}{RT})\bar{\sigma}^5 + [B + A\exp(-\frac{Q}{RT})]\phi\bar{\sigma}^{1.3}$$

$$k = 17.622 + 2.42\times10^{-2}T - 1.696\times10^{-5}T^2, \quad T < 1030\ \mathrm{K}$$

BISON Testing

- BISON can handle binary and ternary fuel and compare reasonably well with EBR-II data
- Discrepancies are due to inadequate knowledge of materials models, and underlying issues with material descriptions, and code robustness
- Development is ongoing, and improvements to swelling models, for example, have been made

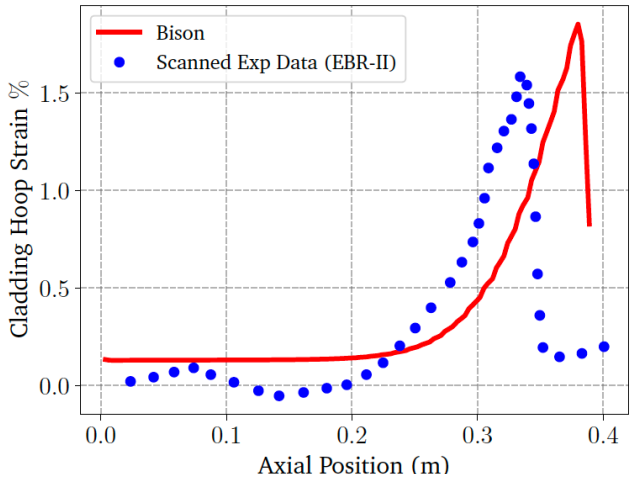

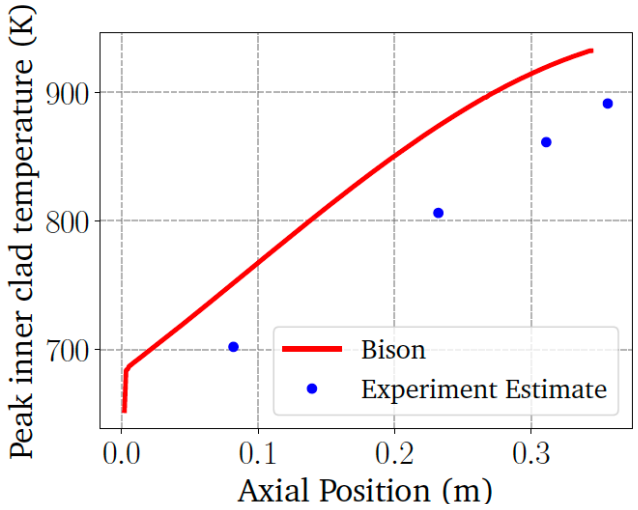

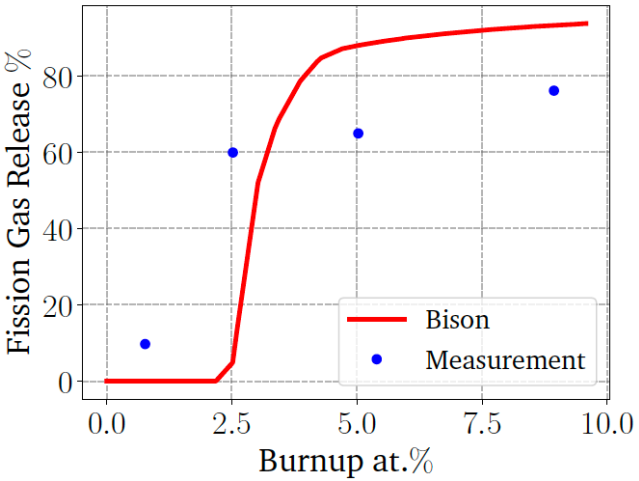

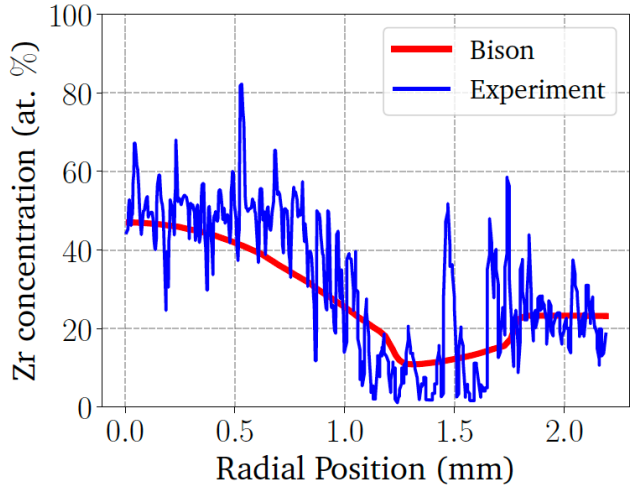

Other Codes

- LIFEMETAL
- The code has evolved from the LIFE series of codes from ANL that perform steady-state and transient analyses for nuclear fuel
- The original code was developed for UO2 and mixed oxide fuels for use in fast reactor systems
- The code was developed in association with the IFR and has been extensively used for planning steady state and transient experiments at EBR-II

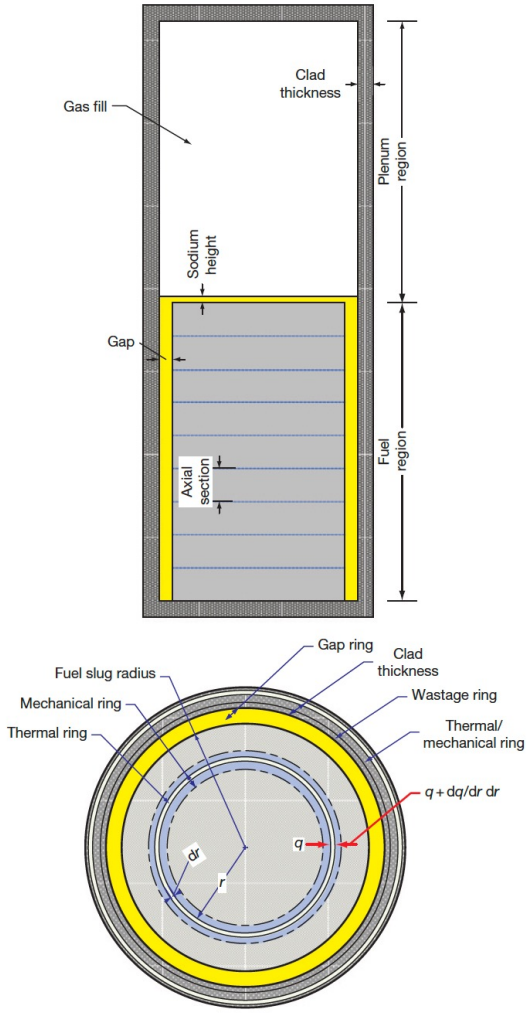

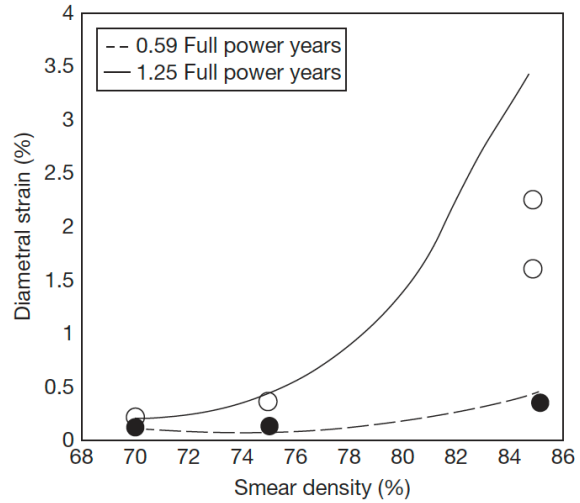

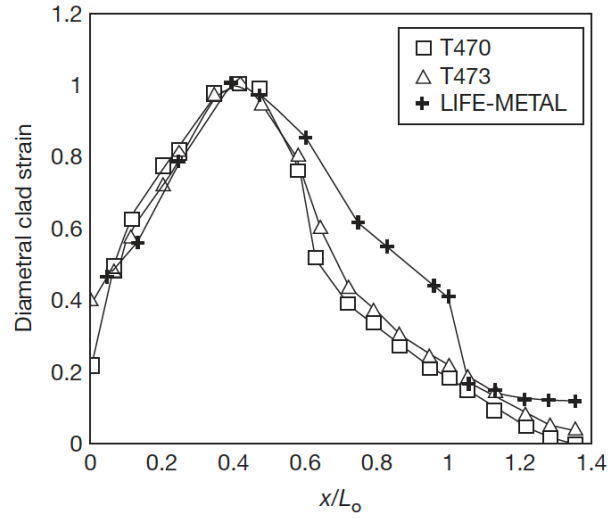

Other Codes

- ALFUS
- JAEA code that is multiphysics in nature and focuses on the mechanical behavior of the fuel under irradiation
- Both LIFE-METAL and ALFUS are capable of simulating metal fuel irradiation behavior to some extent
- Both lack different swelling in different radial zone, coupling of redistribution, realistic predictions of FCCI

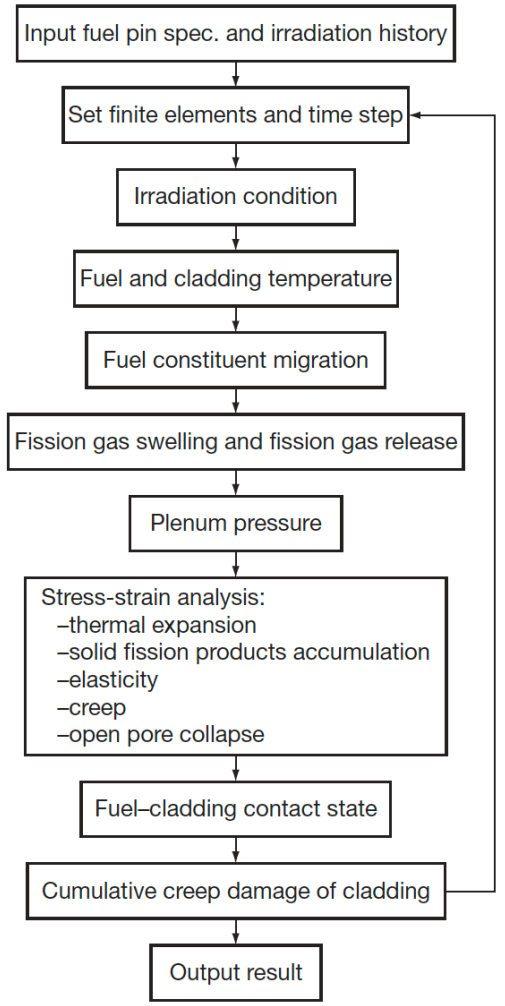

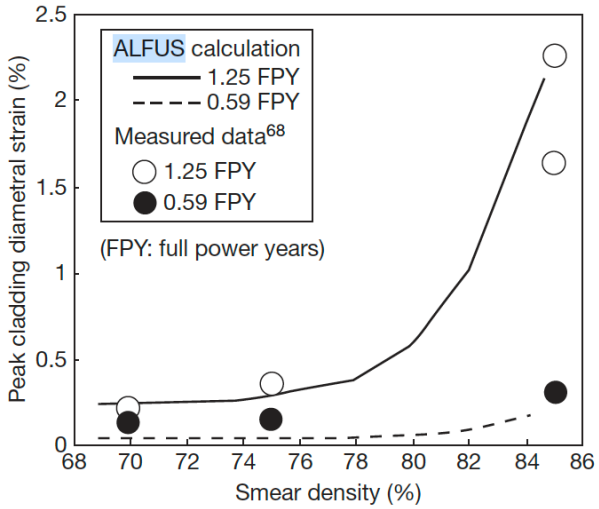

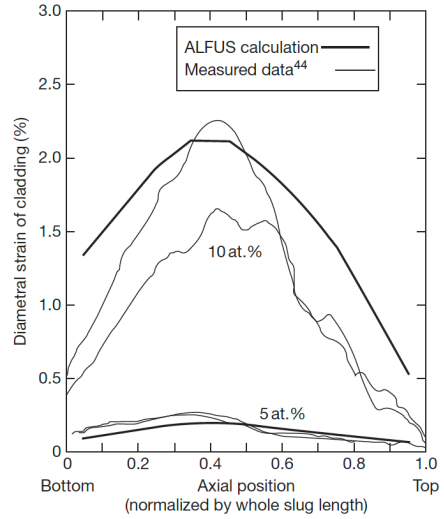

QUESTIONS?